ELSEVIER

Chemical Physics 225 (1997) 77–91

Chemical Physics

The $^{r}Q_1$ branch of carbodiimide, HNCNH, at 1.1 THz [1]

Wolfgang Jabs [a,2], Manfred Winnewisser [a], Sergei P. Belov [b], Thomas Klaus [b], Gisbert Winnewisser [b]

[a] *Physikalisch-Chemisches Institut, Justus-Liebig-Universität, Heinrich-Buff-Ring 58, 35392 Gießen, Germany*
[b] *I. Physikalisches Institut, Universität zu Köln, 50937 Köln, Germany*

Received 5 May 1997

Abstract

The $^{r}Q_1$ branch of the skew-chain molecule HNCNH has been measured at 1.1 THz using a frequency and phase stabilized and continuously tunable backward wave oscillator with a frequency accuracy better than 100 kHz for unblended lines. The newly assigned transitions were added to the existing data base and then fitted to constants of the Watson Hamiltonian in *S*-reduction. The $^{r}Q_1$-branch spectrum is complex because it consists of the superposition of four subbranches resulting from an internal torsional motion through a *trans*- and a *cis*-torsional potential energy barrier of nearly equal height ($\sim 2070\ \mathrm{cm}^{-1}$) and the resolved K_a doubling. As discovered previously, the $K_a = 2$ energy levels in HNCNH are inverted, as in the H_2S_2 and D_2S_2 molecules. This is a consequence of the dominance of the centrifugal-distortion splitting over the pure inertial asymmetry splitting in these accidentally nearly symmetric tops. The contributions of the two effects to the energy levels and to the $^{r}Q_1$-branch transitions have been analysed as well as the J dependence of the torsional splitting. © 1997 Elsevier Science B.V.

1. Introduction

Carbodiimide, HNCNH, is a skew-chain molecule and belongs like H_2S_2 and H_2O_2 to the C_2-symmetry group. Molecules of this type are accidentally nearly symmetric tops; for HNCNH Ray's asymmetry parameter κ was determined to be -0.99999537 [1], for H_2S_2 to be -0.99996081 [2] and for H_2O_2 to be -0.99195922 [3]. The permanent electric dipole moment coincides with the C_2-symmetry axis which is perpendicular to the axis of the least principal moment of inertia. For H_2S_2 and H_2O_2 the symmetry axis coincides with the *c* axis, while for HNCNH the C_2 axis points along the *b* axis. The perpendicular *b*-type rotational spectrum is dominated by strong *Q*-branch absorptions throughout the entire millimeterwave and far infrared region. Additionally each absorption feature is affected by internal rotation of the two H atoms relative to each other hindered by a *trans*- and a *cis*-energy barrier (V_{trans} and V_{cis}). The tunneling motion causes a doubling of each rovibrational energy level [4]. Table 1 gives the torsional potential barrier heights of HNCNH, H_2S_2, and H_2O_2 together with the observed torsional doubling of the rotational transitions. Concerning the torsional splitting of the three molecules, carbo-

[1] This paper is dedicated to Professor Dr. Sigrid D. Peyerimhoff on the occasion of her 60th birthday.

[2] Part of the author's dissertation, Justus-Liebig-Universität Gießen (D26).

PII S0301-0104(97)00175-4

Table 1
Barrier heights of the torsional potential and observed torsional doublet splitting of rotational transitions for H_2S_2, HNCNH, and H_2O_2

Molecule	V_{trans} /cm^{-1}	V_{cis} /cm^{-1}	Observed torsional doublet splitting ($J=0$, $K_a=0$) /MHz
HSSH	2037 [a]	2843 [a]	0.116 [b]
HNCNH	2078 [c]	2061 [c]	467 [d]
HOOH	387 [e]	2563 [e]	685 770 [f]

[a] Ref. [7], [b] Ref. [8], [c] Ref. [5], [d] Ref. [1], [e] Ref. [9], [f] Ref. [3].

diimide is the intermediate case between H_2S_2 and H_2O_2. Therefore it is of interest to record the $^rQ_{K_a}$ branches with high spectral resolution and accuracy.

The *cis*-energy barrier is somewhat smaller than the *trans*-energy barrier for HNCNH, which affects the ordering of the torsional energy levels. Furthermore, the torsional doubling of the rotational lines depends strongly on the rotational quantum number K_a which is indicative of complex internal dynamics compared to H_2S_2 and H_2O_2. In Fig. 1 the magnitude of the observed frequency splitting between the $^rQ_{K_a}$-subbranch centers $|\Delta\nu_c|$ is plotted as a function of K_a. This behaviour indicates that the torsional motion is accompanied by significant skeletal flexing of the HNCNH molecule [5]. The flexibility of the molecule decreases with the rotational excitation and consequently the doublet splitting collapses (Fig. 1). For $K_a \leq 1$ the torsional splitting depends also on the rotational quantum number J.

The rotational torsional spectrum of carbodiimide has been measured in various intervals between 15 GHz and 330 cm^{-1} using a millimeter wave, a submillimeter wave, a laser single-sideband and a high resolution FTIR spectrometer by Birk et al. [1,4]. Recently Wagener et al. [6] resolved the J structure of $^rQ_{K_a}$ branches with $K_a = \{2,3,4\}$ using a tunable far-infrared spectrometer. Now we have been able to complete the data base of the rotational torsional transitions in the vibrational ground state of HNCNH by recording the missing $^rQ_1$ branch with the aid of the Cologne Terahertz Spectrometer.

The present measurements were performed to obtain the spectroscopic information found only in the $^rQ_1$ branches and to study an outstanding spectroscopic feature of carbodiimide, namely the inversion of the energy levels of the K_a-type doublet for $K_a = 2$, which was discovered by Wagener et al. [6]. The inversion of the energy levels is linked to the influence of the $\Delta K_a = \pm 4$ matrix elements in the centrifugal distortion Hamiltonian. This anomalous K_a-type doubling was first detected for the H_2S_2 molecule and its isotopomer D_2S_2 [10,11]. Recently Yamada et al. [12] discussed it in detail. The anomalous K_a-type doubling is a consequence of the fact that the molecules HNCNH, H_2S_2, and H_2O_2 are all very nearly prolate symmetric top rotors for which

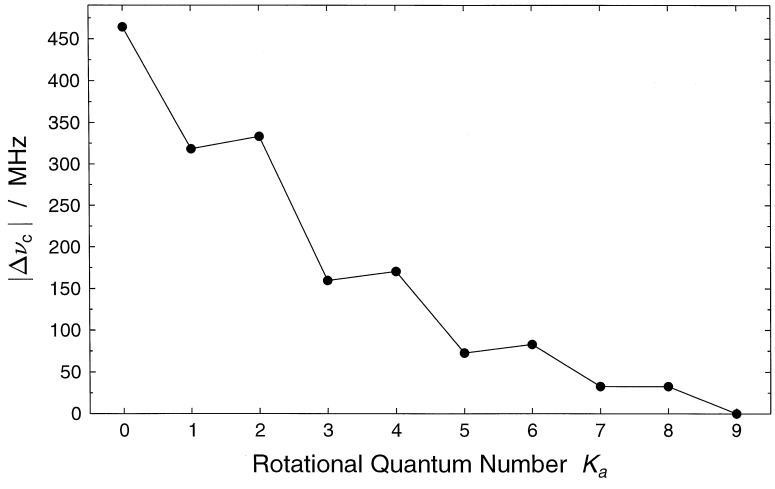

Fig. 1. K_a dependence of the torsional doublet splitting of the $^rQ_{K_a}$ band centers $|\Delta\nu_c|$. Data taken from [1], [6] and this work.

the $\Delta K_a = \pm 2$ matrix elements describing the inertial asymmetry splitting are very small.

2. Experimental details

In essential details the Cologne Terahertz Spectrometer consists of high-frequency, broad-band tunable backward wave oscillators (BWOs) supplied by the ISTOK Research and Production Company, a multiplier/mixer with a low-noise HEMT amplifier circuit, and a tunable millimeter wave KVARZ synthesizer that covers the frequency region 78–118 GHz [13–15]. A block diagram of the spectrometer is shown in Fig. 2. The power output of the high frequency BWO is divided: a small fraction is used to drive the frequency mixer system fed by the output frequency of a KVARZ frequency synthesizer, whereas the major portion of the BWO radiation is focused through the 4 m free space absorption cell and focused onto a He-cooled InSb hot-electron bolometer. Frequencies up to 1.3 THz can be generated with this experimental setup. Source modulation with second derivative detection is used.

Attenuation of the radiation by strong water absorptions is critical in the 1.1 THz region. We therefore had to measure on days with low air humidity, otherwise the power of the high frequency signal was insufficient to drive the frequency mixer system for the phase-lock loop. A sample pressure of 2 Pa was maintained in the cell at room temperature by pumping on a commercial sample of cyanamide, H_2NCN, stabilized with NaH_2PO_4. In the gaseous phase cyanamide is in equilibrium with carbodiimide. At room temperature only $\approx$ 0.25% of the sample exists as carbodiimide [16], so that the partial pressure of carbodiimide was of the order of 0.005 Pa. Consequently the weak spectrum of carbodiimide is overlapped by strong absorption lines of cyanamide. The absolute accuracy of the line positions varies between 100 kHz for strong unblended carbodiimide lines and 300 kHz for weak and partly blended lines. The full linewidth at half maximum (FWHM) of the HNCNH absorption lines is approximately 3 MHz, a value which reflects two roughly equal contributions: Doppler and modulation broadening.

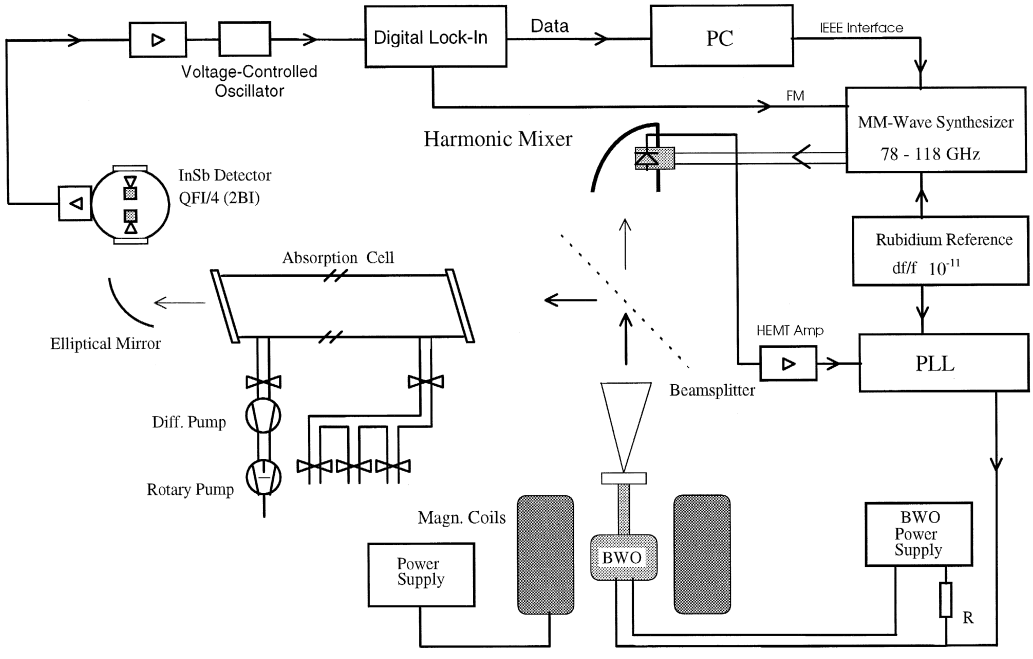

Fig. 2. Block diagram of the Cologne Terahertz Spectrometer.

3. Spectrum, assignment, and fits

An overview spectrum of the $^rQ_1$-branch region is shown in Fig. 3. The strong lines are cyanamide transitions. The appearance of the spectrum is complex because the $^rQ_1$ branch of HNCNH consists of four overlapping subbranches due to the torsional doubling and the K_a-type doubling caused by the inertial asymmetry of the molecule. The torsional motion through *trans*- and *cis*-energy barriers of nearly equal height (Table 1) should result in a splitting of each rotational vibrational energy level into a pair of doublets. Symmetry considerations require, however, that only two of the four torsional rovibrational levels exist: for even K_a the outer torsional rovibrational energy levels exist, which are labeled according to the symmetry designation of the G_4-extended molecular symmetry group A_{1s} and A_{2s}, while for odd K_a the inner torsional rovibrational energy levels exists, which are labeled with A_{1d} and A_{2d} [4]. This is indicated in Fig. 4. The observed torsional splitting for $K_a = 2$ rotational energy levels is thus significantly larger than for $K_a = 1$ energy levels. A_1 denotes the lower torsional level in each case. The torsional selection rules for the perpendicular *b*-type spectrum state that transitions are allowed between A_1- and between A_2-energy levels. The torsional states of H_2S_2 and H_2O_2 are usually labeled with the quantum number τ, $\tau \in \{1,2,3,4\}$, where $\tau = 1$ refers to the A_{1s}, $\tau = 2$ to the A_{2d}, $\tau = 3$ to the A_{1d}, and $\tau = 4$ to the A_{2s} torsional energy levels [7].

An intensity alternation of the rotational torsional lines of HNCNH due to nuclear spin statistics could not be consistently observed in the survey spectrum displayed in Fig. 3. This is in contrast to the $^rQ_0$ and $^rQ_2$ branches, where the intensities of adjacent transitions exhibit spin statistics of 7:5 [4,6]. The lack of directly observable spin statistics is the result of the superposition of the individual absorption lines of the four subbranches, especially for low J. For high J, on the other hand, the intensities become too unreliable to detect unambiguously the relatively small intensity alternation of 7:5. The J assignment of the rotational torsional lines was performed by using an interactive assignment program [17], where

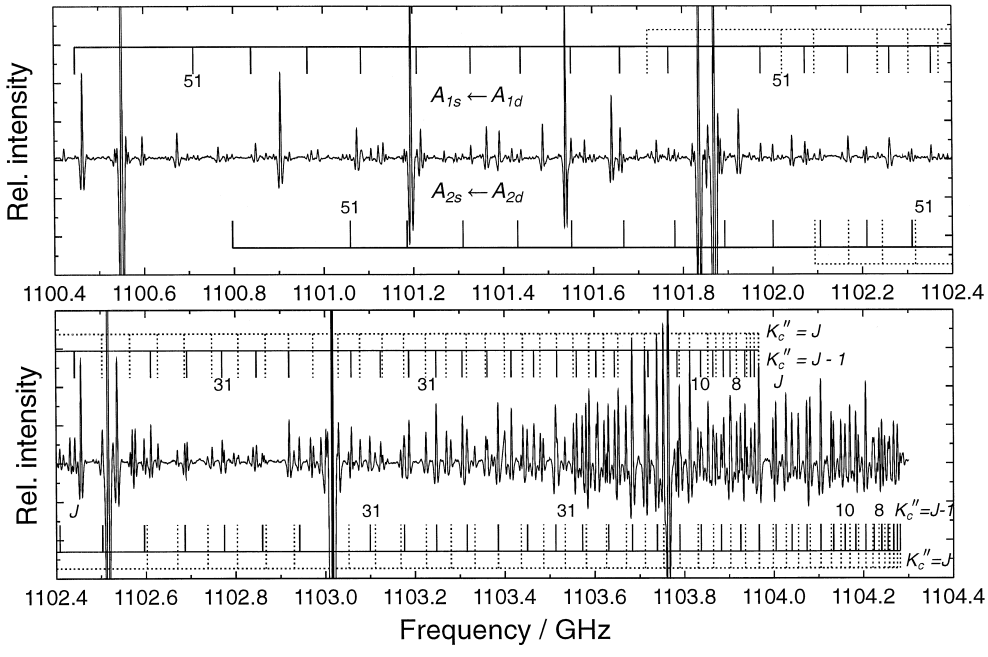

Fig. 3. Survey spectrum of the $^rQ_1$ branch region of carbodiimide. The strong absorption lines are cyanamide transitions. The HNCNH Q branch consists of four subbranches which are due to the torsional and inertial K_a-type doubling. All four subbranches overlap severely.

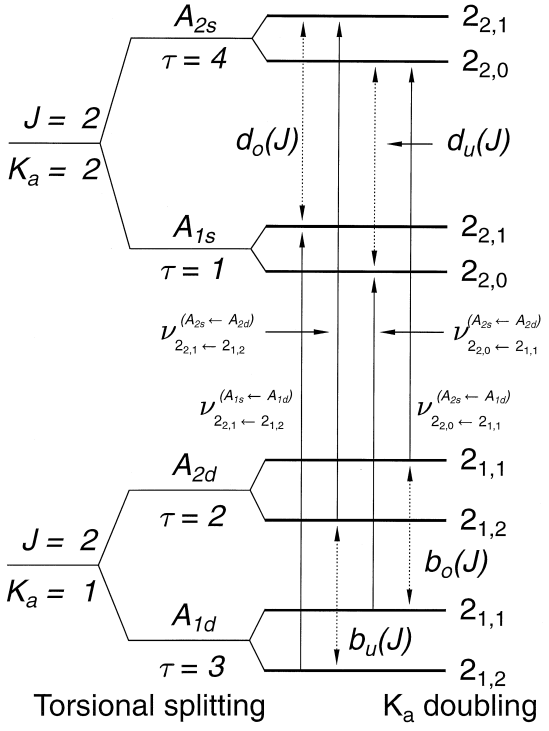

Fig. 4. Schematic term diagram of the lowest $^{r}Q_1$-branch transition of HNCNH. The Q branch consists of four subbranches due to the torsional and the K_a-type doubling. The torsional energy levels can either be labeled according to the G_4-symmetry group or using an additional quantum number τ.

the transition frequencies belonging to a particular subbranch were fitted to a power series (ps) expression in $J(J+1)$:

$$\nu = \nu_c + \Delta B_{ps} J(J+1) - \Delta D_{ps} J^2 (J+1)^2. \qquad (1)$$

Starting values for the power series constants ΔB_{ps} and ΔD_{ps} were derived from the analysis of the mid infrared spectrum of carbodiimide.

All assigned transitions are entered in the Fortrat diagram shown in Fig. 5. Transitions up to $J = 55$ could be assigned. The K_a doubling is resolved for $J \geq 4$. The upper subband head is that of the $A_{2s} \leftarrow A_{2d}$ torsional rotational transitions, while the lower subband head, shifted by 318.3 MHz is that of the $A_{1s} \leftarrow A_{1d}$ transitions. The fitted power series constants are collected in Table 2. All assigned lines together with their deviations from the calculated frequencies are entered in Table 3. Strongly overlapped lines were omitted from the fits.

The new data were added to the existing data base of the rotational torsional transitions measured previously [1,6]. The full data base was divided into two groups of transitions, those of A_1 symmetry and those of A_2 symmetry, which were fitted separately. The transition frequencies are then described by the following formulas [1]:

$$\nu_{A_{1d} \leftrightarrow A_{1s}} = \pm \frac{1}{h} \Big\{ \Delta E_{\text{trans}} + \Big[E_{\text{rot},A_{1d}}(J', K_a', K_c') - E_{\text{rot},A_{1s}}(J'', K_a'', K_c'') \Big] \Big\},$$

$$\nu_{A_{2s} \leftrightarrow A_{2d}} = \pm \frac{1}{h} \Big\{ \Delta E_{\text{trans}} + \Big[E_{\text{rot},A_{2s}}(J', K_a', K_c') - E_{\text{rot},A_{2d}}(J'', K_a'', K_c'') \Big] \Big\}, \qquad (2)$$

with

$$\Delta E_{\text{trans}} = E_{A_{1d}(K_a=0,J=0)} - E_{A_{1s}(K_a=0,J=0)} = E_{A_{2s}(K_a=0,J=0)} - E_{A_{2d}(K_a=0,J=0)}. \qquad (3)$$

This procedure treats each torsional state separately. The transition frequencies consist of two contributions, a torsional part ΔE_{trans} and a rotational part. ΔE_{trans} is the splitting of the energy levels with $J = 0$ and $K_a = 0$ due to the tunneling through the

Table 2
Power series constants fitted to the $^{r}Q_1$-branch transitions of HNCNH

Transition series $J'_{K_a',K_c'} \leftarrow J''_{K_a'',K_c''}$	Torsional symmetry of the lower level	ν_c/GHz	ΔB_{ps}/MHz	ΔD_{ps}/Hz
$J_{2,J-1} \leftarrow J_{1,J}$	A_{1d}	1 103.971 722 (61) [a]	−0.764 07 (12)	−10.917 (41)
$J_{2,J-2} \leftarrow J_{1,J-1}$	A_{1d}	1 103.971 887 (54)	−1.200 00 (11)	11.159 (40)
$J_{2,J-1} \leftarrow J_{1,J}$	A_{2d}	1 104.289 961 (51)	−0.773 22 (11)	−11.208 (40)
$J_{2,J-2} \leftarrow J_{1,J-1}$	A_{2d}	1 104.290 129 (55)	−1.189 02 (11)	11.098 (42)

[a] The numbers in parentheses are one standard deviation in units of the last digit quoted.

Table 3
Assigned $^{r}Q_1$-branch transitions of HNCNH, with $\nu_{obs} - \nu_{calc}$ values calculated with the aid of the spectroscopic constants given in Table 4 (A) and with the aid of the power series constants given in Table 2 (B)

		(A)	(B)			(A)	(B)
$J'_{K'_a,K'_c} \leftarrow J''_{K''_a,K''_c}$	ν_{obs} /MHz	$\nu_{obs} - \nu_{calc}$ /MHz	$\nu_{obs} - \nu_{calc}$ /MHz	$J'_{K'_a,K'_c} \leftarrow J''_{K''_a,K''_c}$	ν_{obs} /MHz	$\nu_{obs} - \nu_{calc}$ /MHz	$\nu_{obs} - \nu_{calc}$ /MHz
Torsional transition: $A_{1s} \leftarrow A_{1d}$							
$2_{2,1} \leftarrow 2_{1,2}$	1 103 966.719	−0.506 *	−0.419 *				
				$3_{2,1} \leftarrow 3_{1,2}$	1 103 956.966	−0.446 *	−0.519 *
$4_{2,3} \leftarrow 4_{1,4}$	1 103 956.966	0.439 *	0.521 *	$4_{2,2} \leftarrow 4_{1,3}$	1 103 948.593	0.781 *	0.711 *
$5_{2,4} \leftarrow 5_{1,5}$	1 103 948.593	−0.296	−0.217	$5_{2,3} \leftarrow 5_{1,4}$	1 103 935.419	−0.389 *	−0.458 *
$6_{2,5} \leftarrow 6_{1,6}$	1 103 939.959	0.233	0.309				
				$7_{2,5} \leftarrow 7_{1,6}$	1 103 902.520	−2.070 *	−2.132 *
$8_{2,7} \leftarrow 8_{1,8}$	1 103 916.759	−0.073	−0.006	$8_{2,6} \leftarrow 8_{1,7}$	1 103 887.743	2.370 *	2.314 *
$9_{2,8} \leftarrow 9_{1,9}$	1 103 902.520	−0.585 *	−0.524 *	$9_{2,7} \leftarrow 9_{1,8}$	1 103 863.977	0.235	0.180
$10_{2,9} \leftarrow 10_{1,10}$	1 103 887.743	−0.119	−0.063	$10_{2,8} \leftarrow 10_{1,9}$	1 103 836.871	−2.830 *	−2.881 *
$11_{2,10} \leftarrow 11_{1,11}$	1 103 871.364	0.260	0.310	$11_{2,9} \leftarrow 11_{1,10}$	1 103 812.510	−0.738 *	−0.783 *
$12_{2,11} \leftarrow 12_{1,12}$	1 103 852.892	−0.057	0.100	$12_{2,10} \leftarrow 12_{1,11}$	1 103 784.161	−0.214	−0.255
				$13_{2,11} \leftarrow 13_{1,12}$	1 103 752.941	−0.142	−0.177
$14_{2,13} \leftarrow 14_{1,14}$	1 103 812.510	0.732 *	0.762 *	$14_{2,12} \leftarrow 14_{1,13}$	1 103 719.517	0.152	0.122
$15_{2,14} \leftarrow 15_{1,15}$	1 103 788.977	−0.020	0.004	$15_{2,13} \leftarrow 15_{1,14}$	1 103 683.376	0.156	0.131
$16_{2,15} \leftarrow 16_{1,16}$	1 103 764.051	−0.667 *	−0.650 *	$16_{2,14} \leftarrow 16_{1,15}$	1 103 644.654	0.012	−0.008
$17_{2,16} \leftarrow 17_{1,17}$	1 103 738.665	−0.282	−0.272	$17_{2,15} \leftarrow 17_{1,16}$	1 103 603.651	0.023	0.008
$18_{2,17} \leftarrow 18_{1,18}$	1 103 711.858	0.169	0.173	$18_{2,16} \leftarrow 18_{1,17}$	1 103 560.258	0.085	0.076
$19_{2,18} \leftarrow 19_{1,19}$	1 103 683.376	0.429 *	0.426 *	$19_{2,17} \leftarrow 19_{1,18}$	1 103 513.512	−0.760 *	2.810 *
$20_{2,19} \leftarrow 20_{1,20}$	1 103 652.800	0.073	0.064	$20_{2,18} \leftarrow 20_{1,19}$	1 103 465.271	−0.649 *	−0.648 *
$21_{2,20} \leftarrow 21_{1,21}$	1 103 620.944	−0.091	−0.106	$21_{2,19} \leftarrow 21_{1,20}$	1 103 415.129	0.018	0.023
$22_{2,21} \leftarrow 22_{1,22}$	1 103 587.897	0.022	0.002	$22_{2,20} \leftarrow 22_{1,21}$	1 103 361.899	0.059	0.068
$23_{2,22} \leftarrow 23_{1,23}$	1 103 553.173	−0.081	−0.106	$23_{2,21} \leftarrow 23_{1,22}$	1 103 306.079	−0.022	−0.009
$24_{2,23} \leftarrow 24_{1,24}$	1 103 517.086	−0.091	−0.121	$24_{2,22} \leftarrow 24_{1,23}$	1 103 247.457	−0.430 *	−0.414 *
$25_{2,24} \leftarrow 25_{1,25}$	1 103 479.557	−0.095	−0.129	$25_{2,23} \leftarrow 25_{1,24}$	1 103 187.111	−0.082	−0.063
$26_{2,25} \leftarrow 26_{1,26}$	1 103 440.723	0.039	0.001	$26_{2,24} \leftarrow 26_{1,25}$	1 103 123.815	−0.195	−0.175
$27_{2,26} \leftarrow 27_{1,27}$	1 103 400.231	−0.050	−0.090	$27_{2,25} \leftarrow 27_{1,26}$	1 103 058.288	−0.046	−0.023
$28_{2,27} \leftarrow 28_{1,28}$	1 103 358.428	−0.021	−0.064				
$29_{2,28} \leftarrow 29_{1,29}$	1 103 316.276	1.080 *	1.036 *	$29_{2,27} \leftarrow 29_{1,28}$	1 102 919.304	−0.163	−0.139
$30_{2,29} \leftarrow 30_{1,30}$	1 103 270.448	−0.083	−0.127	$30_{2,28} \leftarrow 30_{1,29}$	1 102 846.293	0.031	0.055
$31_{2,30} \leftarrow 31_{1,31}$	1 103 224.547	0.087	0.044	$31_{2,29} \leftarrow 31_{1,30}$	1 102 770.449	−0.083	−0.059
$32_{2,31} \leftarrow 32_{1,32}$	1 103 176.113	−0.878 *	−0.920 *	$32_{2,30} \leftarrow 32_{1,31}$	1 102 692.414	0.146	0.168
$33_{2,32} \leftarrow 33_{1,33}$	1 103 128.059	−0.075	−0.115	$33_{2,31} \leftarrow 33_{1,32}$	1 102 611.517	0.054	0.075
$34_{2,33} \leftarrow 34_{1,34}$	1 103 077.843	−0.053	−0.090				
$35_{2,34} \leftarrow 35_{1,35}$	1 103 029.557	3.270 *	3.237 *	$35_{2,33} \leftarrow 35_{1,34}$	1 102 441.858	−0.332 *	−0.316 *
$36_{2,35} \leftarrow 36_{1,36}$	1 102 973.367	0.053	0.023	$36_{2,34} \leftarrow 36_{1,35}$	1 102 353.629	−0.075	−0.063
$37_{2,36} \leftarrow 37_{1,37}$	1 102 919.304	0.314	0.289	$37_{2,35} \leftarrow 37_{1,36}$	1 102 260.431	−2.210 *	−2.200 *
$38_{2,37} \leftarrow 38_{1,38}$	1 102 867.136	3.810 *	3.795 *	$38_{2,36} \leftarrow 38_{1,37}$	1 102 169.063	0.076	0.081
$39_{2,38} \leftarrow 39_{1,39}$	1 102 806.354	0.034	0.020	$39_{2,37} \leftarrow 39_{1,38}$	1 102 072.699	−0.036	−0.036
$40_{2,39} \leftarrow 40_{1,40}$	1 102 748.045	0.049	0.042	$40_{2,38} \leftarrow 40_{1,39}$	1 101 974.004	0.130	0.125
$41_{2,40} \leftarrow 41_{1,41}$	1 102 686.971	−1.390 *	−1.388 *	$41_{2,39} \leftarrow 41_{1,40}$	1 101 869.519	−2.880 *	−2.883 *
$42_{2,41} \leftarrow 42_{1,42}$	1 102 627.443	0.025	0.031	$42_{2,40} \leftarrow 42_{1,41}$	1 101 768.319	0.035	0.023
$43_{2,42} \leftarrow 43_{1,43}$	1 102 565.470	0.284	0.297	$43_{2,41} \leftarrow 43_{1,42}$	1 101 660.850	−0.682 *	−0.697 *
$44_{2,43} \leftarrow 44_{1,44}$	1 102 503.490	1.820 *	1.835 *	$44_{2,42} \leftarrow 44_{1,43}$	1 101 551.955	−0.173	−0.190
				$45_{2,43} \leftarrow 45_{1,44}$	1 101 440.141	0.082	0.063

Table 3 (continued)

$J'_{K'_a,K'_c} \leftarrow J''_{K''_a,K''_c}$	ν_{obs} /MHz	(A) $\nu_{obs}-\nu_{calc}$ /MHz	(B) $\nu_{obs}-\nu_{calc}$ /MHz	$J'_{K'_a,K'_c} \leftarrow J''_{K''_a,K''_c}$	ν_{obs} /MHz	(A) $\nu_{obs}-\nu_{calc}$ /MHz	(B) $\nu_{obs}-\nu_{calc}$ /MHz
$46_{2,45} \leftarrow 46_{1,46}$	1 102 370.607	−0.245	−0.216	$46_{2,44} \leftarrow 46_{1,45}$	1 101 328.957	3.640 *	3.623 *
$47_{2,46} \leftarrow 47_{1,47}$	1 102 303.617	0.051	0.083	$47_{2,45} \leftarrow 47_{1,46}$	1 101 209.003	1.120 *	1.103 *
$48_{2,47} \leftarrow 48_{1,48}$	1 102 235.278	0.231	0.266	$48_{2,46} \leftarrow 48_{1,47}$	1 101 084.629	−3.120 *	−3.135 *
				$49_{2,47} \leftarrow 49_{1,48}$	1 100 964.916	0.012	0.003
$50_{2,49} \leftarrow 50_{1,50}$	1 102 094.106	−0.249	−0.216	$50_{2,48} \leftarrow 50_{1,49}$	1 100 839.272	−0.061	−0.062
$51_{2,50} \leftarrow 51_{1,51}$	1 102 022.069	−0.138	−0.110	$51_{2,49} \leftarrow 51_{1,50}$	1 100 711.070	0.047	0.057
				$53_{2,51} \leftarrow 53_{1,52}$	1 100 447.094	0.957 *	1.001 *
$55_{2,54} \leftarrow 55_{1,55}$	1 101 721.931	0.019	−0.008				
Torsional transition: $A_{2s} \leftarrow A_{2d}$							
				$3_{2,1} \leftarrow 3_{1,2}$	1 104 275.062	−0.728 *	−0.797 *
$4_{2,3} \leftarrow 4_{1,4}$	1 104 275.062	0.469 *	0.560 *	$4_{2,2} \leftarrow 4_{1,3}$	1 104 266.624	0.348	0.280
$5_{2,4} \leftarrow 5_{1,5}$	1 104 266.624	−0.240	−0.151	$5_{2,3} \leftarrow 5_{1,4}$	1 104 254.373	−0.009	−0.076
$6_{2,5} \leftarrow 6_{1,6}$	1 104 257.528	−0.064	0.022	$6_{2,4} \leftarrow 6_{1,5}$	1 104 240.231	0.125	0.060
$7_{2,6} \leftarrow 7_{1,7}$	1 104 246.850	0.071	0.154	$7_{2,5} \leftarrow 7_{1,6}$	1 104 223.273	−0.174	−0.236
$8_{2,7} \leftarrow 8_{1,8}$	1 104 234.337	−0.091	−0.011	$8_{2,6} \leftarrow 8_{1,7}$	1 104 204.821	0.419 *	0.359 *
$9_{2,8} \leftarrow 9_{1,9}$	1 104 220.534	−0.004	0.071	$9_{2,7} \leftarrow 9_{1,8}$	1 104 182.544	−0.426 *	−0.483 *
$10_{2,9} \leftarrow 10_{1,10}$	1 104 204.821	−0.294	−0.222	$10_{2,8} \leftarrow 10_{1,9}$	1 104 158.913	−0.235	−0.290
$11_{2,10} \leftarrow 11_{1,11}$	1 104 188.369	0.210	0.277	$11_{2,9} \leftarrow 11_{1,10}$	1 104 133.022	0.088	0.037
$12_{2,11} \leftarrow 12_{1,12}$	1 104 169.549	−0.126	−0.063	$12_{2,10} \leftarrow 12_{1,11}$	1 104 104.631	0.307	0.259
$13_{2,12} \leftarrow 13_{1,13}$	1 104 149.481	−0.184	−0.126	$13_{2,11} \leftarrow 13_{1,12}$	1 104 073.162	−0.153	−0.198
$14_{2,13} \leftarrow 14_{1,14}$	1 104 127.944	−0.188	−0.136	$14_{2,12} \leftarrow 14_{1,13}$	1 104 039.884	−0.020	−0.062
$15_{2,14} \leftarrow 15_{1,15}$	1 104 104.631	−0.451 *	−0.403 *	$15_{2,13} \leftarrow 15_{1,14}$	1 104 004.073	−0.014	−0.052
$16_{2,15} \leftarrow 16_{1,16}$	1 104 080.559	0.041	0.084	$16_{2,14} \leftarrow 16_{1,15}$	1 103 966.719	0.859 *	0.824 *
$17_{2,16} \leftarrow 17_{1,17}$	1 104 054.302	−0.141	−0.104	$17_{2,15} \leftarrow 17_{1,16}$	1 103 925.177	−0.042	−0.073
$18_{2,17} \leftarrow 18_{1,18}$	1 104 026.896	0.032	0.065	$18_{2,16} \leftarrow 18_{1,17}$	1 103 881.929	−0.229	−0.257
$19_{2,18} \leftarrow 19_{1,19}$	1 103 997.700	−0.084	−0.057	$19_{2,17} \leftarrow 19_{1,18}$	1 103 836.871	0.197	0.172
$20_{2,19} \leftarrow 20_{1,20}$	1 103 966.719	−0.490 *	−0.467 *	$20_{2,18} \leftarrow 20_{1,19}$	1 103 788.977	0.215	0.194
$21_{2,20} \leftarrow 21_{1,21}$	1 103 935.419	0.275 *	0.293 *	$21_{2,19} \leftarrow 21_{1,20}$	1 103 738.665	0.250	0.232
$22_{2,21} \leftarrow 22_{1,22}$	1 103 902.520	0.925 *	0.938 *	$22_{2,20} \leftarrow 22_{1,21}$	1 103 683.376	−2.250 *	−2.268 *
$23_{2,22} \leftarrow 23_{1,23}$	1 103 863.977	−2.590 *	−2.582 *	$23_{2,21} \leftarrow 23_{1,22}$	1 103 630.415	0.020	0.006
$24_{2,23} \leftarrow 24_{1,24}$	1 103 830.110	0.041	0.045	$24_{2,22} \leftarrow 24_{1,23}$	1 103 572.639	−0.072	−0.083
$25_{2,24} \leftarrow 25_{1,25}$	1 103 788.977	−3.130 *	−3.127 *	$25_{2,23} \leftarrow 25_{1,24}$	1 103 513.512	0.944 *	0.934 *
$26_{2,25} \leftarrow 26_{1,26}$	1 103 752.941	0.258	0.256	$26_{2,24} \leftarrow 26_{1,25}$	1 103 450.024	0.063	0.056
$27_{2,26} \leftarrow 27_{1,27}$	1 103 711.858	0.049	0.045	$27_{2,25} \leftarrow 27_{1,26}$	1 103 385.159	0.278	0.271
$28_{2,27} \leftarrow 28_{1,28}$	1 103 669.571	0.081	0.074	$28_{2,26} \leftarrow 28_{1,27}$	1 103 316.276	−1.056 *	−1.052 *
$29_{2,28} \leftarrow 29_{1,29}$	1 103 625.688	−0.047	−0.056	$29_{2,27} \leftarrow 29_{1,28}$	1 103 247.457	0.180	0.175
$30_{2,29} \leftarrow 30_{1,30}$	1 103 580.850	0.299 *	0.289 *	$30_{2,28} \leftarrow 30_{1,29}$	1 103 176.113	1.380 *	1.370 *
$31_{2,30} \leftarrow 31_{1,31}$	1 103 534.007	0.061	0.050	$31_{2,29} \leftarrow 31_{1,30}$	1 103 099.539	−0.157	−0.162
$32_{2,31} \leftarrow 32_{1,32}$	1 103 486.056	0.127	0.116				
$33_{2,32} \leftarrow 33_{1,33}$	1 103 436.254	−0.253	−0.264	$33_{2,31} \leftarrow 33_{1,32}$	1 102 941.984	−0.088	−0.094
$34_{2,33} \leftarrow 34_{1,34}$	1 103 385.159	−0.532 *	−0.543 *	$34_{2,32} \leftarrow 34_{1,33}$	1 102 859.266	−0.207	−0.214
$35_{2,34} \leftarrow 35_{1,35}$	1 103 333.466	−0.023	−0.032	$35_{2,33} \leftarrow 35_{1,34}$	1 102 774.413	0.076	0.067
$36_{2,35} \leftarrow 36_{1,36}$	1 103 279.948	0.038	0.030	$36_{2,34} \leftarrow 36_{1,35}$	1 102 686.971	0.316	0.306
$37_{2,36} \leftarrow 37_{1,37}$	1 103 224.547	−0.418 *	−0.424 *	$37_{2,35} \leftarrow 37_{1,36}$	1 102 596.347	−0.071	−0.082
$38_{2,37} \leftarrow 38_{1,38}$	1 103 168.320	−0.342 *	−0.346 *	$38_{2,36} \leftarrow 38_{1,37}$	1 102 503.490	−0.124	−0.138
$39_{2,38} \leftarrow 39_{1,39}$	1 103 111.109	0.096	0.095	$39_{2,37} \leftarrow 39_{1,38}$	1 102 408.153	−0.083	−0.098
$40_{2,39} \leftarrow 40_{1,40}$	1 103 051.785	−0.242	−0.241	$40_{2,38} \leftarrow 40_{1,39}$	1 102 310.236	−0.036	−0.052
				$41_{2,39} \leftarrow 41_{1,40}$	1 102 209.706	−0.005	−0.023

Table 3 (continued)

$J'_{K'_a,K'_c} \leftarrow J''_{K''_a,K''_c}$	ν_{obs} /MHz	(A) $\nu_{obs}-\nu_{calc}$ /MHz	(B) $\nu_{obs}-\nu_{calc}$ /MHz	$J'_{K'_a,K'_c} \leftarrow J''_{K''_a,K''_c}$	ν_{obs} /MHz	(A) $\nu_{obs}-\nu_{calc}$ /MHz	(B) $\nu_{obs}-\nu_{calc}$ /MHz
$42_{2,41} \leftarrow 42_{1,42}$	1 102 929.998	−0.092	−0.084	$42_{2,40} \leftarrow 42_{1,41}$	1 102 106.497	−0.046	−0.066
$43_{2,42} \leftarrow 43_{1,43}$	1 102 867.136	−0.024	−0.014	$43_{2,41} \leftarrow 43_{1,42}$	1 102 000.720	−0.037	−0.058
$44_{2,43} \leftarrow 44_{1,44}$	1 102 803.158	0.220	0.233	$44_{2,42} \leftarrow 44_{1,43}$	1 101 892.518	0.176	0.156
$45_{2,44} \leftarrow 45_{1,45}$	1 102 737.689	0.254	0.268	$45_{2,43} \leftarrow 45_{1,44}$	1 101 781.300	0.014	−0.005
$46_{2,45} \leftarrow 46_{1,46}$	1 102 670.464	−0.200	−0.184	$46_{2,44} \leftarrow 46_{1,45}$	1 101 667.809	0.232	0.214
$47_{2,46} \leftarrow 47_{1,47}$	1 102 602.494	−0.142	−0.126	$47_{2,45} \leftarrow 47_{1,46}$	1 101 551.955	0.752 *	0.737 *
				$48_{2,46} \leftarrow 48_{1,47}$	1 101 432.012	−0.140	−0.151
				$49_{2,47} \leftarrow 49_{1,48}$	1 101 310.435	0.023	0.019
				$50_{2,48} \leftarrow 50_{1,49}$	1 101 185.786	−0.183	−0.179
$51_{2,50} \leftarrow 51_{1,51}$	1 102 317.981	−0.231	−0.227	$51_{2,49} \leftarrow 51_{1,50}$	1 101 058.790	−0.021	−0.007
$52_{2,51} \leftarrow 52_{1,52}$	1 102 244.057	−0.036	−0.040				
$53_{2,52} \leftarrow 53_{1,53}$	1 102 169.063	0.268	0.253	$53_{2,51} \leftarrow 53_{1,52}$	1 100 796.406	0.111	0.154
$54_{2,53} \leftarrow 54_{1,54}$	1 102 094.106	1.770 *	1.745 *				

* Lines marked by an asterisk were not included in the fit.

trans-energy barrier. This torsional part should be equal for both sets of levels. The energy splitting ΔE_{cis} caused by the tunneling trough the *cis*-energy barrier can not be determined directly due to the selection rules.

For describing the rotational contribution, we used

Table 4
Effective spectroscopic constants of the Watson Hamiltonian in *S*-reduction, describing the rotational torsional transitions of HNCNH in the vibrational ground state

Constant		Symmetry of the torsional levels A_{1s}	A_{1d}	A_{2s}	A_{2d}
A	/MHz	379 266.812(26) [a]	379 247.131(58)	379 221.454(22)	379 239.763(49)
B	/MHz	10 366.955 1(18)	10 366.953 4(20)	10 366.928 2(16)	10 366.929 8(16)
C	/MHz	10 366.084 3(20)	10 366.082 6(18)	10 366.097 3(18)	10 366.098 9(18)
D_J	/kHz	3.245 9(13)	3.245 8(13)	3.246 1(14)	3.246 1(14)
D_{JK}	/kHz	326.772(26)	326.498(24)	324.720(21)	325.044(20)
D_K	/MHz	169.791 1(52)	168.872 3(87)	167.265 2(45)	168.025 9(75)
d_1	/Hz	−5.64(11)	−5.64(11)	−5.46(10)	−5.46(10)
d_2	/Hz	−16.937(18)	−16.937(18)	−16.797(16)	−16.797(16)
H_{KJ}	/Hz	−173.1(35)	−173.1(35)	−369.1(30)	−369.1(30)
H_K	/kHz	457.90(34)	438.77(39)	385.78(29)	399.87(34)
h_1	/mHz	−0.051(28)	−0.051(28)	−0.037(27)	−0.037(27)
L_{KJ}	/Hz	9.74(17)	9.81(17)	1.38(15)	1.27(15)
L_K	/kHz	1.903 3(62)	1.770 1(63)	0.990 1(54)	1.078 8(54)
S_{KJ}	/mHz	94.5(31)	94.5(31)	−33.7(27)	−33.7(27)
S_K	/Hz	5.427(34)	5.427(34)	1.383(29)	1.383(29)
T_{KJ}	/mHz	0.769(18)	0.769(18)	0.144(16)	0.144(16)
$(\Delta E_{trans}/h)$	/MHz	229.347(57)	229.347(57)	227.717(49)	227.717(49)
σ	/kHz	208	208	185	185

[a] The numbers in parentheses are one standard deviation in units of the last digit quoted.

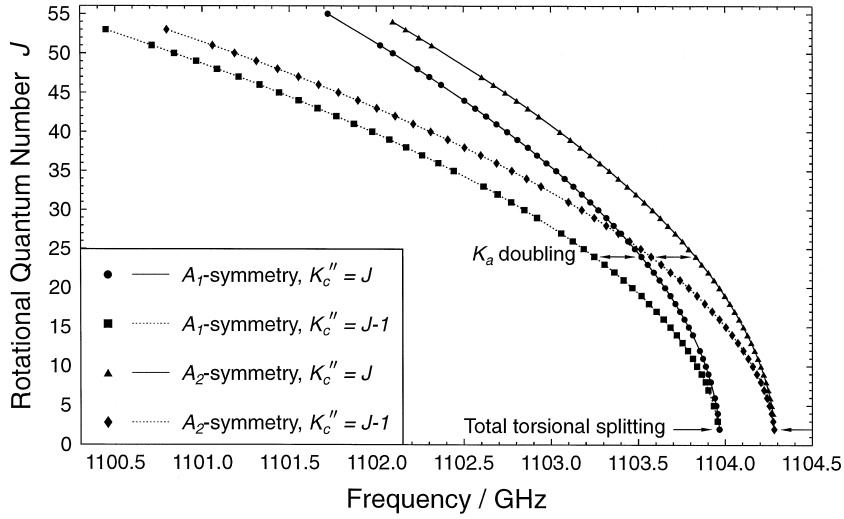

Fig. 5. Fortrat diagram of assigned $^rQ_1$ lines of HNCNH, indicating the four subbranches.

the Watson Hamiltonian in *S*-reduction [18,19]. The matrix elements in the basis of the prolate symmetric top wavefunctions $|J,K_a\rangle$, including the constants relevant to this work, are as follows:

$$\begin{aligned}\frac{E_{K_a,K_a}}{h} &= \tfrac{1}{2}(B+C)J(J+1)\\ &\quad+\left[A-\tfrac{1}{2}(B+C)\right]K_a^2-D_J J^2(J+1)^2\\ &\quad-D_{JK}J(J+1)K_a^2-D_K K_a^4\\ &\quad+H_{KJ}J(J+1)K_a^4+H_K K_a^6\\ &\quad-L_{KJ}J(J+1)K_a^6-L_K K_a^8\\ &\quad+S_{KJ}J(J+1)K_a^8+S_K K_a^{10}\\ &\quad-T_{KJ}J(J+1)K_a^{10}, \qquad (4)\end{aligned}$$

$$\begin{aligned}\frac{W_{K_a,K_a\pm 2}}{h} &= \tfrac{1}{4}\left[(B-C)+d_1J(J+1)+h_1J^2(J+1)^2\right]\\ &\quad\times\{f(J,K_a,0)f(J,K_a,1)\}, \qquad (5)\end{aligned}$$

$$\frac{V_{K_a,K_a\pm 4}}{h} = d_2\prod_{l=0}^{3}f(J,K_a,l), \qquad (6)$$

with

$$f(J,K_a,l)=\sqrt{J(J+1)-(K_a\pm l)(K_a\pm l\pm 1)}\,. \qquad (7)$$

A, *B* and *C* are rotational constants, while all other constants are centrifugal distortion constants. The constants obtained are given in Table 4 for the four torsional states. The combined analysis of the present data with the earlier measurements reported in Refs. [1,6] yielded 52 effective spectroscopic constants which were fitted to 515 transitions between A_1 torsional levels and 524 transitions between A_2 torsional levels. The deviations of the resulting calculated frequencies from the experimental frequencies measured in this work are included in Table 3.

In order to confirm the assignment, which was not possible directly using the nuclear spin statistics due to the problems discussed above, we simulated the four $^rQ_1$ subbranches using the adjusted constants of the effective Hamiltonian given in Table 4. The observed and simulated spectra in the region of the two bandheads are shown in Fig. 6. The linewidth of an individual rotational torsional line is determined by Doppler and modulation broadening, the latter is caused by the source modulation. For simulating the spectrum we assumed a Voigt line-profile function subjected to modulation broadening by using the formulas given by Bayer-Helms and Helmcke [20]. In order to reproduce the line shapes satisfactorily, we optimized the values for the modulation amplitude (3.4 MHz), assuming a pure sine wave modulation and second derivative detection and the FWHM of the Lorentz contribution (1.6 MHz) on a single unblended line. However, these are effective parame-

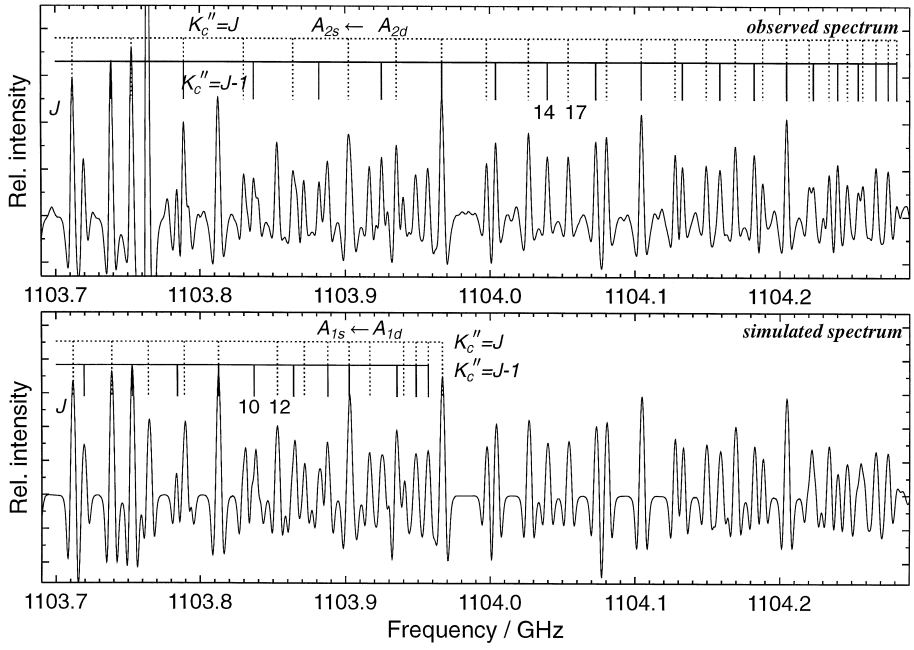

Fig. 6. Observed and simulated spectrum of the ${}^{r}Q_1$ branch of HNCNH in the region of the two bandheads. The specific assignment comb gives the symmetry notation and the J-values of the individual line positions.

ters, since the source modulation is not necessarily a pure sine wave.

4. Discussion of the fits

The previously published fits of the rotational torsional transitions in the vibrational ground state of carbodiimide by Birk et al. [1] and Wagener et al. [6] differ substantially in the A rotational constant and in the torsional constant ΔE_{trans}, leading to predictions for the ${}^{r}Q_1$-branch transitions which differ by as much as 40 MHz in the line positions. Adding the newly assigned lines of Table 3 to the previously published data and making a somewhat different choice of centrifugal distortion constants (several more constants were adjusted separately for each symmetry species), we were able to obtain a set of adjusted constants which are in agreement with the values given by Birk et al. [1].

The two values of $\Delta E_{\text{trans}}/h$ determined by the fits of the A_1 and A_2 torsional symmetry levels differ only by 1.63 MHz. This is an improvement compared with the previous fits (3.79 MHz by Birk et al. and 7.99 MHz by Wagener et al.), but the two values for $\Delta E_{\text{trans}}/h$ are still not equal, as would be expected from theory. This might be caused by the fact that the torsional motion produces a weak J-dependence which is absorbed in centrifugal-distortion constants.

The only higher order centrifugal constant which is poorly defined in the present fit is h_1. However, this constant is needed to describe the high J ${}^{r}Q_1$-branch transitions satisfactorily.

5. Analysis of the K_a-type doubling

Winnewisser [10,11] had shown that for accidentally nearly symmetric top molecules two contributions to the K_a-type doubling of the rovibrational levels are important: The inertial asymmetry splitting, which can be considered to be a $\Delta K_a = \pm 2$ interaction, and the centrifugal-distortion splitting, caused by the $\Delta K_a = \pm 4$ interaction matrix element in the asymmetric top Hamiltonian. With the spectroscopic constants obtained for the Watson Hamiltonian in S-reduction we can now analyse the influ-

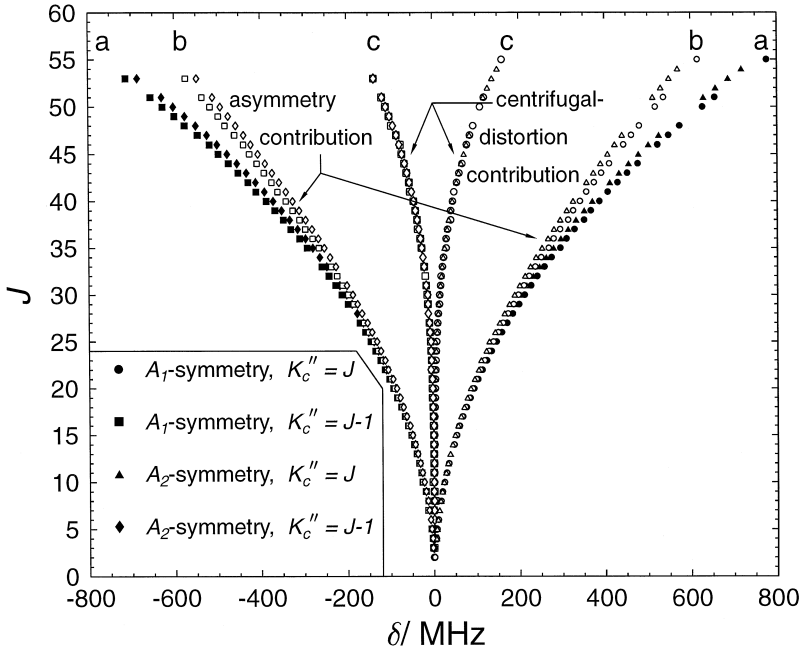

Fig. 7. The K_a-type doubling of the ${}^rQ_1$-branch transitions of HNCNH. Case (a) gives the observed doubling as the difference between two δ values with the same J, case (b) gives the $\Delta K_a = \pm 2$ asymmetry contribution and case (c) the $\Delta K_a = \pm 4$ centrifugal distortion contribution to the doubling. δ represents the difference between the observed transition frequency ν_{obs} and a modeled frequency ν_{mod}.

ence of each contribution on the K_a-type doubling of the ${}^rQ_1$-branch transitions separately. We define the quantity $\delta = \nu_{\text{obs}} - \nu_{\text{mod}}$ as the difference between the observed transition frequency ν_{obs} and a set of modeled frequencies ν_{mod} which are calculated for several cases, taking into account the various interactions:

(a) ν_{mod} is calculated with the $\Delta K_a = \pm 2$ and $\Delta K_a = \pm 4$ matrix elements fixed to zero, so that ν_{mod} represents the transition frequency in the symmetric top approximation. The difference of two δ values for the same J and K_a'' quantum numbers is thus equal to the observed K_a-type doubling of the transitions.

(b) ν_{mod} is calculated with the $\Delta K_a = \pm 2$ matrix elements fixed to zero; it contains, however, the $\Delta K_a = \pm 4$ centrifugal distortion contribution to the K_a-type doubling of the transitions. In this case δ reflects the inertial asymmetry contribution to the doubling.

(c) ν_{mod} is calculated with the $\Delta K_a = \pm 4$ matrix elements fixed to zero; retaining the $\Delta K_a = \pm 2$ inertial asymmetry contribution to the K_a-type doubling of the transitions. In this case δ reflects the centrifugal-distortion contribution to the doubling.

Fig. 7 shows the J dependence of the δ values calculated for the ${}^rQ_1$ branch for the three cases. It can be seen that the centrifugal-distortion contribution becomes enhanced with increasing J. This is a consequence of the fact that the doubling of the $K_a = 2$ levels, which is dominated by the $\Delta K_a = \pm 4$ interaction contribution, increases more rapidly with J than the doubling of the $K_a = 1$ levels, which is caused mainly by the $\Delta K_a = \pm 2$ interaction contribution. The J dependence of the $V_{K_a, K_a \pm 4}/h$ matrix element is of higher order compared to that of the leading term of the matrix element $W_{K_a, K_a \pm 2}/h$ given in Eqs. (5) and (6). To illustrate this K_a and J dependence Fig. 8 shows the reduced term values F_{red}, defined as in Wagener et al. [6] as $F_{\text{red}} = F - F_{\text{mod}}$, plotted against J. The term values F were calculated with all constants given in Table 4, and the modeled term values F_{mod} according to the cases given above and specified in the Fig. 7. The domi-

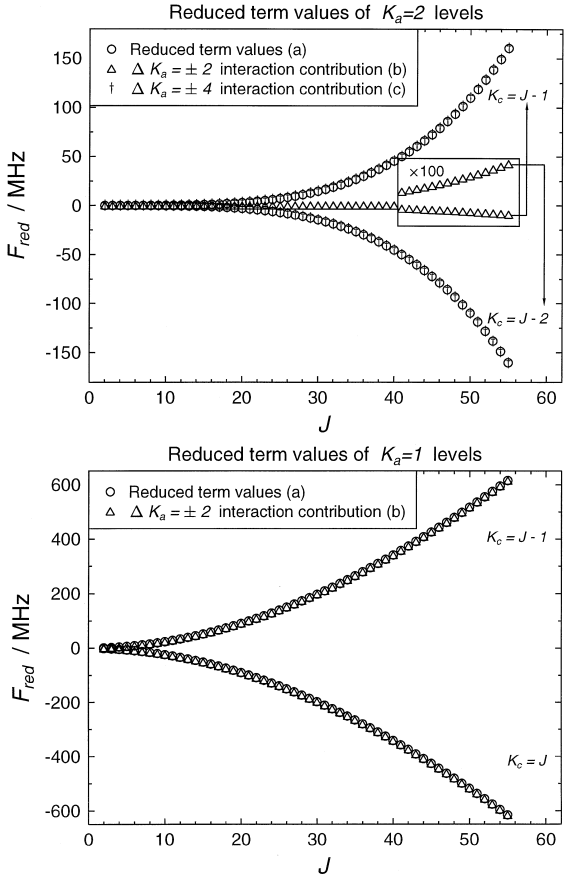

Fig. 8. Reduced term values of the $K_a = 1$ and $K_a = 2$ rotational levels of HNCNH calculated for the A_1-symmetry torsional state.

nant contribution of the centrifugal-distortion for the $K_a = 2$ doublet leads to an inversion of the order of the energy levels, as was determined by Wagener et al. [6].

6. *J* Dependence of the torsional splitting

Birk et al. [1] examined the J dependence of the torsional doublet splitting exhibited by the ${}^rQ_0$- and the ${}^rP_0/{}^pR_1$-branch transitions, the only transitions where a significant J dependence of the doublet splitting could be detected. The analysis at that time, which had to rely on an assumption, led to the conclusion that the torsional energy separation of the upper levels of the asymmetry doublet shows a linear dependence on $J(J+1)$ while the torsional energy separation of the lower levels of the asymmetry doublet is nearly independent of J.

Fig. 9 shows the J dependence of the torsional splitting derived from the ${}^rQ_1$-branch transitions listed in Table 3. For both asymmetry components of the K_a doublet the torsional doublet splitting shows a dependence on J which is linear with $J(J+1)$, of a similar order of magnitude as that observed for the ${}^rQ_0$ branch [1]. The scatter in Fig. 9 is a consequence of the fact that for many lines at least one component of the torsional doublet is overlapped by an interfering line.

No J dependence of the torsional doublet splitting was observed for the ${}^rQ_2$-branch transitions [6]. With this information we can analyse the J dependence of the torsional energy separation of the $K_a = 1$ levels according to the formalism of Birk et al. [1]. Therefore we define the differences between the energy levels of the torsional doublet with $K_a = 0,1$ and 2 as follows:

$$
\begin{aligned}
a(J) &= \left[E_{A_{2s}}(0,J) - E_{A_{1s}}(0,J)\right], \\
b_u(J) &= \left[E_{A_{2d}}(1,J) - E_{A_{1d}}(1,J)\right]_u, \\
b_o(J) &= \left[E_{A_{2d}}(1,J) - E_{A_{1d}}(1,J)\right]_o, \\
d_u(J) &= \left[E_{A_{2s}}(2,J) - E_{A_{1s}}(2,J)\right]_u, \\
d_o(J) &= \left[E_{A_{2s}}(2,J) - E_{A_{1s}}(2,J)\right]_o, \qquad (8)
\end{aligned}
$$

where the index u refers to $K_c = J - K_a + 1$ for $K_a = 1$ and $K_c = J - K_a$ for $K_a = 2$ and the index o refers to $K_c = J - K_a$ for $K_a = 1$ and $K_c = J - K_a + 1$ for $K_a = 2$. With these definitions and referring to Fig. 4 we can write the equations

$$
\begin{aligned}
\nu^{(A_{2s} \leftarrow A_{2d})}_{J_{2,J-2} \leftarrow J_{1,J-1}} + b_o(J) &= \nu^{(A_{1s} \leftarrow A_{1d})}_{J_{2,J-2} \leftarrow J_{1,J-1}} + d_u(J), \\
\nu^{(A_{2s} \leftarrow A_{2d})}_{J_{2,J-1} \leftarrow J_{1,J}} + b_u(J) &= \nu^{(A_{1s} \leftarrow A_{1d})}_{J_{2,J-1} \leftarrow J_{1,J}} + d_o(J). \qquad (9)
\end{aligned}
$$

We can then define the doublet splitting

$$\Delta\nu_D = \nu^{(A_{2s} \leftarrow A_{2d})} - \nu^{(A_{1s} \leftarrow A_{1d})} \qquad (10)$$

and for the observed doublet splitting of the ${}^rQ_1$ branch we then have

$$
\begin{aligned}
\Delta\nu_D(J_{2,J-2} \leftarrow J_{1,J-1}) &= d_u(J) - b_o(J), \\
\Delta\nu_D(J_{2,J-1} \leftarrow J_{1,J}) &= d_o(J) - b_u(J). \qquad (11)
\end{aligned}
$$

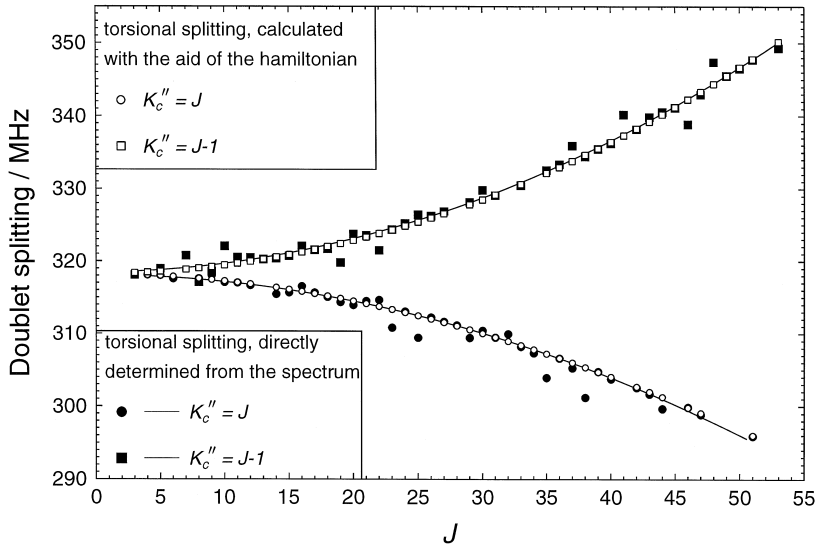

Fig. 9. J dependence of the torsional doublet splitting of the ${}^rQ_1$-branch transitions. The filled markers represent the values directly determined from the assigned lines, the open markers are the values determined with the fitted constants of the Hamiltonian. The scatter of the filled markers are caused by the fact that at least one component of the doublet is perturbed by another line.

For the ${}^rQ_0$ branch, as shown by Birk et al. [1], we have analogously

$$\Delta\nu_D(J_{1,J-1} \leftarrow J_{0,J}) = a(J) - b_o(J). \tag{12}$$

For the overall change of the energy separation with J, defined as $\delta X(J) = X(J) - X(0)$, whereby $X(J)$ stands for a J dependent quantity, we obtain

$$\delta b_o(J) = \delta d_u(J) - \delta\left[\Delta\nu_D(J_{2,J-2} \leftarrow J_{1,J-1})\right],$$
$$\delta b_u(J) = \delta d_o(J) - \delta\left[\Delta\nu_D(J_{2,J-1} \leftarrow J_{1,J})\right]. \tag{13}$$

The doublet splitting of the ${}^rQ_2$-branch transitions, as noted above, does not show a J dependence within the experimental error [6]. This means that the total variation of the torsional doublet splitting shown by the ${}^rQ_2$-branch transitions is smaller than 500 kHz in the observed range of $J = 4$ to $J = 42$. This leads to the conclusion that both δd_u and δd_o are zero. The observed J dependence of the torsional splitting of the ${}^rQ_1$-branch transition is than only determined by the J dependence of the $K_a = 1$ energy levels. For these we obtain the following results from the J dependence of the ${}^rQ_1$-branch transitions:

$K_c'' = J$:

$$\Delta\nu_D(J) = 317.88(28)\ \text{MHz} - 8.77(25) \times 10^{-3}\ \text{MHz}\ J(J+1),$$

$K_c'' = J-1$:

$$\Delta\nu_D(J) = 318.36(29)\ \text{MHz} + 11.12(21) \times 10^{-3}\ \text{MHz}\ J(J+1), \tag{14}$$

and in terms of the coefficients c_{b_o} and c_{b_u} we have

$$\delta b_o(J) = -\delta\left[\Delta\nu_D(J_{2,J-2} \leftarrow J_{1,J-1})\right] = c_{b_o}J(J+1) = -11.12(21)\ \text{kHz}\ J(J+1),$$
$$\delta b_u(J) = -\delta\left[\Delta\nu_D(J_{2,J-1} \leftarrow J_{1,J})\right] = c_{b_u}J(J+1) = 8.77(25)\ \text{kHz}\ J(J+1). \tag{15}$$

Thus, this analysis yields a linear dependence on $J(J+1)$ of the same order of magnitude, but oppo-

site sign, for the torsional energy separations of the upper levels and the lower levels of the asymmetry doublet. Birk et al. [1] obtained for $\delta b_o(J) = -19.157(42)$ kHz $J(J+1)$ and for $\delta b_u \approx 0$ kHz. The substantial difference between the values in this work and the values published previously is due to the fact that Birk et al. tried to determine three constants from two equations. The coefficient describing δb_u in one of these equations was assumed to be zero, because it was shown that this term should exhibit a linear $J(J-1)$ dependence whereas the observed torsional doublet splitting $\delta[\Delta\nu_{DP}(J)]$ of the ${}^rP_0$-branch transitions could be fitted to an expression linear in $J(J+1)$:

$$\begin{aligned}\delta\left[\Delta\nu_{DP}(J)\right] &= c_a J(J+1) - c_{b_u} J(J-1)\\ &= (c_a - c_{b_u})J^2 + (c_a + c_{b_u})J\\ &\approx -13.907(34)\ \text{kHz}\ J(J+1).\end{aligned} \tag{16}$$

We found that the observed doublet $\Delta\nu_{DP}(J)$ splitting of the ${}^rP_0$-branch transitions can also be fitted just as well as a function of J^2:

$$\delta\left[\Delta\nu_{DP}(J)\right] = -14.307(40)\ \text{kHz}\ J^2. \tag{17}$$

A linear coefficient in J could not be determined from the fifteen ${}^rP_0$-branch transitions. Eq. (16) would then be fulfilled with $c_a \approx -c_{b_u} \neq 0$. Using then Eqs. (15) and (17) we obtain $c_a = -5.54(25)$ kHz. From the J dependence of the torsional splitting of the ${}^rQ_0$-branch transitions [1],

$$\begin{aligned}\delta\left[\Delta\nu_{DQ}(J)\right] &= c_a J(J+1) - c_{b_o} J(J+1)\\ &= 5.249(25)\ \text{kHz}\ J(J+1),\end{aligned} \tag{18}$$

and Eq. (15) we have $c_a = -5.87(21)$ kHz. We thus have now directly determined the J dependence of the torsional splitting for both the $K_a = 0$ and $K_a = 1$ levels. The splitting of the two asymmetry components for $K_a = 1$ are seen to have opposite and roughly equivalent J dependence.

7. Conclusions

By adding newly assigned ${}^rQ_1$-branch transitions to the existing data base of rotational torsional transitions of HNCNH in the vibrational ground state, we obtained more detailed and reliable spectroscopic constants which are in good agreement with those of Birk et al. [1]. Accurate rotational constants are needed to determine the structure of HNCNH, a work which is now in progress. The effects determining the K_a doubling of the ${}^rQ_1$-branch transitions were analysed. Further, the J dependence of the torsional rotational doublet splitting was unambiguously determined for $K_a = 0$ and both asymmetry components of the $K_a = 1$ levels.

Acknowledgements

The authors thank B.P. Winnewisser for many helpful discussions during the analysis of the data and for critically reading the manuscript. W. Jabs thanks the Studienstiftung des deutschen Volkes for a scholarship and the members of the Cologne submillimeter wave laboratory for their friendly collaboration. The work in Gießen was supported in part by the Deutsche Forschungsgemeinschaft, the Fonds der Chemischen Industrie and the Max-Planck research award, while the work in Cologne was supported in part by the Deutsche Forschungsgemeinschaft via Grant SFB 301 and special funding from the Science Ministry of the Land Nordrhein-Westfalen.

References

[1] M. Birk, M. Winnewisser, E.A. Cohen, J. Mol. Spectrosc. 136 (1989) 402.
[2] J. Behrend, P. Mittler, G. Winnewisser, K.M.T. Yamada, J. Mol. Spectrosc. 150 (1991) 99.
[3] P. Helminger, W.C. Bowman, F.C. DeLucia, J. Mol. Spectrosc. 85 (1981) 120.
[4] M. Winnewisser, M. Birk, J. Chem. Soc., Faraday Trans. (2) 84 (1988) 1341.
[5] P. Pracna, M. Winnewisser, B.P. Winnewisser, J. Mol. Spectrosc. 162 (1993) 127.
[6] V. Wagener, M. Winnewisser, M. Bellini, J. Mol. Spectrosc. 170 (1995) 323.
[7] S. Urban, E. Herbst, P. Mittler, G. Winnewisser, K.M.T. Yamada, M. Winnewisser, J. Mol. Spectrosc. 137 (1989) 327.
[8] E. Herbst, G. Winnewisser, Chem. Phys. Lett. 155 (1989) 572.
[9] J.-M. Flaud, C. Camy-Peyret, J.W.C. Johns, B. Carli, J. Chem. Phys. 91 (1989) 1504.

[10] G. Winnewisser, J. Chem. Phys. 56 (1972) 2944.
[11] G. Winnewisser, J. Chem. Phys. 57 (1972) 1803.
[12] K.M.T. Yamada, J. Behrend, S.P. Belov, G. Winnewisser, J. Mol. Spectrosc. 176 (1996) 397.
[13] G. Winnewisser, A.F. Krupnov, M.Yu. Tretyakov, M. Liedtke, F. Lewen, A.H. Saleck, R. Schieder, A.P. Shkaev, S.A. Volokhov, J. Mol. Spectrosc. 165 (1994) 294.
[14] G. Winnewisser, Vib. Spectrosc. 8 (1995) 241.
[15] S.P. Belov, F. Lewen, Th. Klaus, G. Winnewisser, J. Mol. Spectrosc. 174 (1995) 606.
[16] M. Birk, Ph.D. Thesis, Justus-Liebig-Universität, Gießen (1988).
[17] F. Stroh, M. Winnewisser, B.P. Winnewisser, J. Mol. Spectrosc. 162 (1993) 435.
[18] J.K.G. Watson, J. Chem. Phys. 46 (1967) 1935.
[19] J.K.G. Watson, J. Chem. Phys. 48 (1968) 4517.
[20] F. Bayer-Helms, J. Helmcke, PTB-Bericht Me-17 (1977) 85.